

Relic gravitational waves: latest revisions and preparations for new data

Wen Zhao^{1,2} and L. P. Grishchuk^{1,3}

¹*School of Physics and Astronomy, Cardiff University, Cardiff, CF24 3AA, United Kingdom*

²*Wales Institute of Mathematical and Computational Sciences, Swansea, SA2 8PP, United Kingdom*

³*Sternberg Astronomical Institute, Moscow State University, Moscow, 119899, Russia*

(Dated: November 5, 2018)

The forthcoming release of data from the Planck mission, and possibly from the next round of Wilkinson Microwave Anisotropy Probe (WMAP) observations, make it necessary to revise the evaluations of relic gravitational waves in the existing data and, at the same time, to refine the assumptions and data analysis techniques in preparation for the arrival of new data. We reconsider with the help of the commonly used CosmoMC numerical package the previously found indications of relic gravitational waves in the 7-year (WMAP7) data. The CosmoMC approach reduces the confidence of these indications from approximately 2σ level to approximately 1σ level, but the indications do not disappear altogether. We critically analyze the assumptions that are currently used in the cosmic microwave background (CMB) data analyses and outline the strategy that should help avoid the oversight of relic gravitational waves in the future CMB data. In particular, it is important to keep away from the unwarranted assumptions about density perturbations. The prospects of confident detection of relic gravitational waves by the Planck satellite have worsened, but they are still good. It appears that more effort will be required in order to mitigate the foreground contamination.

I. INTRODUCTION

Cosmology relies on extrapolations. It is natural to extrapolate the picture of approximate homogeneity and isotropy seen in our patch of the Universe to other places and times. Having assumed the usual framework of a homogeneous and isotropic hot big bang, we do not encounter any real contradictions or paradoxes requiring drastic solutions. But we do encounter an initial cosmological singularity [1]. The singularity is not an ultimate answer, it is only a sign of limited applicability of the currently available theories. The limit of applicability is probably set by the Planck parameters. It seems logical to suggest that our Universe came into being as a configuration with a Planckian size and a Planckian energy density, and with a total energy, including gravity, equal to zero (see [2] and references therein).

It is here where a real problem arises. The newly created classical configuration cannot reach the averaged energy density and size of the presently observed Universe, unless the configuration experienced a kind of primordial kick. During the kick the size of the newly born Universe (for simplicity, one can think of the curvature radius of a closed universe) should increase by many orders of magnitude without significant changes in the energy density of the whatever substance that was there. Such an expansion cannot be driven by normal types of matter which we presently know. The kick should be driven by something more exotic: a lucky version of a scalar field (inflaton) [3] or something like a conformal anomaly [4] or something from the “theory of everything”.

The strong variable gravitational field of the very early Universe inevitably generates gravitational waves and, under certain extra conditions, density perturbations and rotational perturbations [5]. The generating mechanism is the superadiabatic (parametric) amplification of the

zero-point quantum oscillations of the respective degrees of freedom, or, in more technical terms, the Schrodinger evolution of the initial vacuum (ground) state of the corresponding time-dependent Hamiltonian into a strongly squeezed vacuum (multiparticle) quantum state [5]. The generated gravitational waves and density perturbations leave observable imprints in the temperature and polarization anisotropies of the cosmic microwave background radiation. By studying the CMB correlation functions TT , TE , EE , BB we can learn about the birth of the Universe and the initial stage of cosmological expansion.

The simplest assumption about the initial kick is that its entire duration can be described by the scale factor with one fixed power-law dependence [5]:

$$a(\eta) = l_o|\eta|^{1+\beta}, \quad (1)$$

where l_o and β are constants, $\beta < -1$. Then, the generated primordial spectra of metric perturbations describing gravitational waves (t) and density perturbations (s) (for more explanations, see [6]) have the universal power-law forms

$$P_t(k) = A_t \left(\frac{k}{k_0}\right)^{n_t}, \quad P_s(k) = A_s \left(\frac{k}{k_0}\right)^{n_s-1}, \quad (2)$$

where we will be using $k_0 = 0.002\text{Mpc}^{-1}$. According to the theory of quantum-mechanical generation of cosmological perturbations [5] the spectral indices are approximately equal, $n_s - 1 = n_t = 2(\beta + 2)$, and the amplitudes $(A_t)^{1/2}$ and $(A_s)^{1/2}$ are of the order of magnitude of the ratio H_i/H_{Pl} , where $H_i \sim c/l_o$ is the characteristic value of the Hubble parameter during the kick.

The presently available CMB and large-scale structure observations cover a huge interval of scales, ranging from wave numbers $k \approx 0.0002\text{Mpc}^{-1}$ and up to $k \approx 0.2\text{Mpc}^{-1}$. There is no any particularly fundamental reason why a single power-law evolution (1) should

be valid during a long interval of time and, consequently, exact power-law spectra (2) valid in the interval of wavelengths where the ends of the spectrum differ from each other by a factor 10^3 . We do not know such spectra in physics and astrophysics. In cosmology, one can also expect some deviations from strict power-laws (2) [7], [8].

If the continuous power spectrum can be approximated by two power-law pieces, one can write

$$P_s(k) = A_s^{(1)} \left(\frac{k}{k_0} \right)^{n_s^{(1)}-1}, \quad k < k_1, \quad (3)$$

$$P_s(k) = A_s^{(2)} \left(\frac{k}{k_0} \right)^{n_s^{(2)}-1}, \quad k > k_1, \quad (4)$$

where $A_s^{(2)} = A_s^{(1)} \left(\frac{k_1}{k_0} \right)^{n_s^{(1)}-n_s^{(2)}}$, and

$$P_t(k) = A_t^{(1)} \left(\frac{k}{k_0} \right)^{n_t^{(1)}}, \quad k < k_1, \quad (5)$$

$$P_t(k) = A_t^{(2)} \left(\frac{k}{k_0} \right)^{n_t^{(2)}}, \quad k > k_1, \quad (6)$$

where $A_t^{(2)} = A_t^{(1)} \left(\frac{k_1}{k_0} \right)^{n_t^{(1)}-n_t^{(2)}}$.

Obviously, we return to Eq.(2) if the spectral indices in the two pieces are equal to each other.

Alternatively, one can postulate a simple law of “running” of the spectral index,

$$n_s(k) = n_s(k_0) + \alpha_s \ln(k/k_0), \quad (7)$$

where α_s is a constant. The spectral index $n_s(k) - 1$ for density perturbations is defined as $n_s(k) - 1 = [d \ln P_s(k)/d \ln k]$, and similar definition is used for $n_t(k)$. Then the power spectrum for density perturbations takes the form

$$P_s(k) = A_s(k_0) \left(\frac{k}{k_0} \right)^{n_s(k_0)-1+\frac{1}{2}\alpha_s \ln(k/k_0)}, \quad (8)$$

and a similar formula holds for gravitational waves. In our calculations below we will be testing both options, (3)-(4) and (7), of spectral deviations.

Following the (quite unfortunate) tradition, we are characterizing the amount of relic gravitational waves (GW) by ratios involving density perturbations (DP), rather than by the gravitational wave amplitudes directly. One measure is the quadrupole ratio

$$R \equiv \frac{C_{\ell=2}^{TT}(\text{gw})}{C_{\ell=2}^{TT}(\text{dp})}, \quad (9)$$

another – the so-called tensor-to-scalar ratio

$$r \equiv \frac{A_t(k_0)}{A_s(k_0)}. \quad (10)$$

By definition, r and R cannot be negative. Some elements of numerical software are better adjusted to one

quantity than to another. We will be using both of them remembering that $r \approx 2R$ for a quite wide class of models [6].

Contrary to the theory of quantum-mechanical generation of cosmological perturbations, the inflationary theory claims that the power spectrum of density perturbations should be many orders of magnitude larger than the power spectrum of gravitational waves. The inflationary theory attempts to apply to density perturbations the same mechanism of superadiabatic (parametric) amplification that was originally worked out for gravitational waves [5]. But the so-called classic result of inflationary theory states that the A_s should be arbitrarily large in the limit of de Sitter inflation (i.e. when the perturbations are generated with spectral indices $n_s = 1$ and $n_t = 0$): $A_s \approx A_t/\epsilon$, where $\epsilon \equiv -\dot{H}/H^2$ is zero for de Sitter expansion with any Hubble parameter H (i.e. for any “energy scale of inflation”). The existence and properties of primordial density perturbations are consequences of the quantum-mechanical generating mechanism, and not of the inflationary theory. The contribution of inflationary theory to this subject is the (incorrect) prediction of divergent A_s , that is, the (incorrect) prediction of amplitudes that can be arbitrarily larger than H_i/H_{Pl} . For inflationary considerations about density perturbations, see for example [9] and recent books on cosmology.

Inflationists rarely suffer from the problem of “too little”, they usually have the fine-tuning trouble because they generate “too much”. They have started from the threat to “overclose the Universe” and they continue this trend till now. To make the wrong theory look “consistent”, inflationists convert their prediction of arbitrarily large A_s into the prediction of arbitrarily small A_t . As a result, the most advanced string-based inflationary theories predict the negligibly small amounts of gravitational waves, $r \approx 10^{-24}$ or less. In other words, inflationists attempt to pay by gravitational waves for their incorrect treatment of density perturbations. (For a more detailed criticism of inflationary theory, see the last paper in [5].) Obviously, we do not accept the inflationary theory. We allow the use of the inflationary “consistency relation” $r = -8n_t$ only in Sec.II where we repeat the derivations of the WMAP Collaboration [10], [11] who used this relation.

The previous search [6] for relic gravitational waves in the WMAP data was based on the simplified likelihood function which, among other things, neglects the data and noise correlations at the lowest multipoles. The approaching release of data from the Planck mission [12] and, possibly, from the next round of WMAP observations, makes it necessary to test by other numerical techniques the previously found indications of relic gravitational waves. The WMAP team and other groups routinely employ the CosmoMC software [13]. The data analysis constructions in [6] are based on the genuine Wishart probability density function, whereas the WMAP likelihood function, as a part of CosmoMC package, is based on semi-Gaussian approximations to

this distribution. The new analysis with CosmoMC is certainly different from the previous one, but we are reluctant to say that it is necessarily more accurate from the physical point of view. However, we realize that the CosmoMC code is the approach that most of the groups are pursuing now and will be using in the future with new data. Therefore, it is important to revise the previous evaluations of relic gravitational waves with the help of CosmoMC, and to make revised forecasts for Planck observations. This is the main purpose of this paper.

In Sec.II we rederive the results of WMAP Collaboration [10], [11] using their assumptions and methods. In Sec.III we apply the CosmoMC package to repeat the previously performed search for relic GW at lower- ℓ multipoles [6]. We show that the indications of GW diminish but do not disappear altogether. In Sec.IV we demonstrate that the conclusions about n_s and r depend on the interval of multipoles utilized in the data analysis. It is unwise to postulate constant spectral indices in a huge interval of accessible wavelengths and multipoles. In Sec.V we explore a hypothesis of primordial spectra consisting of two power-law pieces. It is shown that the hypothesis is consistent with the data and with the results discussed in previous Sections. Sec.VI is devoted to refined forecasts for the Planck mission. The prospects of confident detection of relic gravitational waves by Planck are still reasonable.

II. REPEATING THE WMAP7 ANALYSIS

First of all, with the help of CosmoMC, we repeat the WMAP7 calculations. We want to be sure that we obtain the same results when we make the same assumptions. Obviously, we include gravitational waves from the very beginning, we do not consider the “minimal” model of WMAP [10] where gravitational waves are voluntarily excluded from the outset. In Sec. IIA, the spectral indices are assumed strictly constant in the entire interval of relevant wavelengths, that is, together with the WMAP team, we adopt Eq.(2). In Sec. IIB, we allow for the “running” of n_s , that is, together with WMAP, we use Eq.(7). Moreover, in these two subsections, and only there, instead of the correct relation $n_t = n_s - 1$, we use the incorrect “consistency relation” $n_t = -r/8$ for reducing the number of unknown parameters. This is done exclusively because the WMAP team has done this, and we want to rederive their results. Since r cannot be negative, the inflationary theory does not allow positive n_t .

A. Constant spectral indices

We repeat the WMAP team analysis of the 7-year CMB data with the help of the CosmoMC sampler. The space of free parameters subject to evaluation consists of four background parameters ($\Omega_b h^2$, $\Omega_c h^2$, τ , θ) and three

perturbation parameters ($\ln(10^{10} A_s)$, n_s , r). These are the standard CosmoMC parameters for a flat Λ CDM cosmology. As mentioned, we also adopt Eq.(2) and atop of that, $n_t = -r/8$. We call this set of assumptions the *Case I*.

The analysis takes into account the observed CMB data for all four angular power spectra: TT , TE , EE and BB [14]. The range of the used multipoles is $2 \leq \ell \leq \ell_{\max}$, where $\ell_{\max} = 1200$ for TT spectrum, 800 for TE spectrum, and 23 for EE and BB spectra. The maximum likelihood values and marginalized distributions are found for all seven free parameters, but we are showing the results only for n_s and r because we are mostly interested in them.

The results of the CosmoMC calculations for the *Case I* are summarized in the upper row of Table I and in Fig. 1. The seven-dimensional (7d) ML values of n_s and r are shown in the column “Maximum likelihood”. The one-dimensional (1d) marginalized distributions for n_s and r are shown in Fig. 1 by olive curves, marked also by symbol (1). (The maximum of 1d likelihoods is always normalized to 1.) The obtained results are very close to the WMAP findings [10]. We see that the assumptions of the *Case I* lead to the conclusion that the primordial spectrum is red, $n_s < 1$. Although the uncertainties are still large, the $n_s < 1$ is the preferred outcome of the WMAP analysis [10] and of our repetition here under the same assumptions. The $n_s < 1$ would mean that the function $P_s(k)$ is infra-red divergent at very small wavenumbers k . The maximum likelihood (ML) values of r , both, for the 7d and 1d posterior distributions, are very close to zero. The 95% confidence limit $r \approx 0.38$ is usually interpreted as the upper limit for the possible amount of relic gravitational waves.

B. Running spectral index

Here, together with the WMAP Collaboration, we increase the number of free parameters from seven to eight by adding the parameter α_s and adopting Eq.(7). We call this set of assumptions the *Case II*. Other parameters, observational data, and CosmoMC numerical techniques are exactly the same as in the *Case I*. The parameter α_s does not have to be a nonzero number. It is the maximum likelihood analysis of the data that determines its value.

The results of the analysis for the *Case II* are shown in the lower row of Table I and in Fig. 1. The eight-dimensional (8d) ML values of $n_s(k_0)$, α_s and r are shown in the column “Maximum likelihood”. The posterior 1d distributions of $n_s(k_0)$ and r are plotted by magenta curves, marked also by symbol (2).

Together with the WMAP team, we see that the primordial spectrum in the *Case II* becomes blue at long wavelengths, that is, the 8d and 1d ML values of $n_s(k_0)$ are larger than 1. The power spectrum $P_s(k)$ is no longer divergent at very small k . Since the ML α_s is negative,

the spectrum gradually turns over from the blue at long wavelengths to red, $n_s(k) < 1$, at shorter wavelengths, see also Eq.(7). There is a considerable decrease of $n_s(k)$ on the way from the long-wavelength end of the spectrum at $k \approx 0.0002\text{Mpc}^{-1}$ to the short-wavelength end of the spectrum at $k \approx 0.2\text{Mpc}^{-1}$. (We restrain from a discussion of disastrous consequences that the values $n_s(k) \geq 1$ bring forth to the inflationary theory.)

In comparison with the *Case I*, the 1d distribution of r becomes significantly broader, and it is almost flat at small values of r , where $r \in (0, 0.12)$. The 8d ML value of r is $r = 0.06$. This value is 7.5 times larger than that in the *Case I*, but one should take this number with caution. When the distribution is almost flat, the ML point can be accidental. It is clear from the shape of the magenta curve in Fig. 1 that the assumptions of the *Case II* are consistent with the hypothesis of no gravitational waves, $r = 0$. Nevertheless, the probability of large values of r has increased, as compared with the *Case I*. The 95% C.L. has risen up to $r \approx 0.43$.

III. EVALUATIONS OF RELIC GRAVITATIONAL WAVES FROM LOWER- ℓ CMB DATA

The purpose of this Section is to revise by the CosmoMC code the previously found indications of relic gravitational waves [6] in the WMAP7 data. It was stressed many times [6], [15] that the relic GW compete with density perturbations only at relatively small multipoles ℓ . It is dangerous to include high- ℓ CMB data in the search for gravitational waves, as the spectral indices may not be constant. Conclusions about the amount of relic gw in the interval $2 \leq \ell \leq 100$ depend on the contribution of density perturbations to these multipoles, but the assessment about the participating A_s and n_s may be wrong, if it is built on the hypothesis of constant spectral indices in a huge interval of the observed multipoles. The relatively small number of data points in the interval $2 \leq \ell \leq 100$ brings forth the increased uncertainty in the evaluation of relic GW, but it seems to be wiser to live with larger uncertainty (and wait for better data) than with artificial certainty based on wrong assumptions.

The arguments put forward in [6], as well as the results of Sec.IIB, hint at possible deviations of the underlying spectra of primordial perturbations from strict power-laws. We perform a special investigation of this issue in Sec.IV.

No doubt, in a search for relic GW, one should always check for the presence of residual systematic effects and alternative explanations. The lower- ℓ multipoles attract attention for a variety of reasons, including purely instrumental deficiencies, and they all should be examined (see, for example, [16], [17], [18]). The helpful signatures of gravitational waves are a nonzero B-mode of CMB polarization [19] and a negative TE cross-correlation at lower multipoles [20].

In Sec.III A we make exactly the same assumptions as in [6], including the fixed best-fit values of the background parameters. But the new results for the perturbation parameters A_s , n_s and r follow from the CosmoMC technique rather than from the procedure of Ref.[6]. We generalize this search in Sec.III B where the background parameters are not fixed but are derived together with the perturbation parameters. For this purpose we use the CosmoMC facility allowing to combine external data, not affecting the perturbation parameters, with the CMB data at $2 \leq \ell \leq 100$.

A. Fixed background parameters

To work exactly with the same assumptions as in Ref.[6], we fix the background parameters at their best-fit values of Λ CDM cosmology [10]: $\Omega_b h^2 = 0.02260$, $\Omega_c h^2 = 0.1123$, $\Omega_\Lambda = 0.728$, $\tau = 0.087$. The Hubble constant $h = 0.704$ is a derived parameter. The free parameters subject to evaluation by the CosmoMC code are $\ln(10^{10} A_s)$, n_s and r . The spectral indices are related by $n_t = n_s - 1$. The CMB data are used only up to $\ell_{\text{max}} = 100$. We call this set of assumptions the *Case III*.

There exists some awkwardness in our choice of the background parameters, as these are the parameters that were derived by the WMAP team [10] under the assumptions of complete absence of gravitational waves and strictly constant n_s in the entire interval of participating wavelengths. We know from our previous experience [6] that the background parameters, if changed not too much, do not greatly affect the results for the perturbation parameters. Nevertheless, for safety, we explicitly explore the issue of background parameters, and allow them to vary, in the more general approach of Sec.III B. This will remove the aforementioned awkwardness in choosing and fixing the background parameters.

By running the CosmoMC code, we find the following 3d ML values of the perturbation parameters r , n_s and $\ln(10^{10} A_s)$:

$$r = 0.285, \quad n_s = 1.052, \quad \ln(10^{10} A_s) = 3.023, \quad (11)$$

and $n_t = 0.052$. We also derived the marginalized 1d results for these parameters (see also Table II),

$$n_s = 1.064_{-0.059}^{+0.058}, \quad \ln(10^{10} A_s) = 2.996_{-0.112}^{+0.108}. \quad (12)$$

Following the convention of [10], we quote here and below the mean values of the 1d likelihood functions, and the uncertainties refer to the 68% confidence intervals. The 1d likelihood functions for n_s and r are plotted by red lines, also marked by (3), in the upper and lower panels of Fig. 1, respectively.

The red curve in the lower panel shows a clearly visible broad maximum at $r = 0.2$. Unfortunately, the peak point $r = 0.2$ is not strongly separated from $r = 0$, it is nearly (slightly less than) 1σ away from $r = 0$. Speaking

TABLE I: Results for n_s , α_s and r in Case I and Case II

	Maximum likelihood			1-d likelihood		
	n_s	α_s	r	n_s	α_s	r (95%C.L.)
Case I	0.967	...	0.008	$0.991^{+0.021}_{-0.020}$...	$r < 0.379$
Case II	1.061	-0.043	0.060	$1.065^{+0.058}_{-0.058}$	$-0.039^{+0.029}_{-0.026}$	$r < 0.430$

more accurately, the 68% and 95% areas under the probability curve are covered, respectively, by the following intervals of the parameter r :

$$r \in (0, 0.452) \quad \text{and} \quad r \in (0, 0.843), \quad (13)$$

so that the point $r = 0$ (barely) belongs to the 68% interval.

The 3d ML values, $n_s = 1.052$ and $r = 0.285$, obtained with CosmoMC are smaller than those found in our previous work [6], $n_s = 1.111$ and $R = 0.264$ (which is equivalent to $r = 0.550$), in exactly the same setting. At the same time, the ML value of A_s is larger than before. Physically, this means that the new analysis indicates a larger contribution of density perturbations and a smaller contribution of gravitational waves. The outcome $r = 0.285$ in (11) is almost a factor of 2 smaller than the previous number $r = 0.550$. Taken for the face value, these new evaluations weaken the indications of relic gravitational waves in the WMAP7 data from approximately a 2σ level to approximately a 1σ level. This also worsens the prospects of confident detection of relic GW by the Planck satellite (more details in Sec.VI). Nevertheless, it is fair to say that some qualitative indications of blue spectral indices, and possibly of a large amount of gravitational waves, have survived.

It is unclear to us why the CosmoMC numerical technique has led to a factor of 2 grimmer results for r than the previous analysis in [6]. It does not seem likely that this happened because of a better treatment of noises. The increased noises would probably lead only to a larger spread of likelihood functions, but this does not seem to be the case. The difference is more like a systematic shift of ML points for r by a factor of 2 toward smaller values of r . More work is needed in order to understand the cause of this discrepancy.

B. Varied background parameters

To alleviate the worries about fixed background parameters, we run the CosmoMC option allowing to find the background parameters together with the perturbation parameters. The information on the background parameters is provided by the widely quoted external data (not affecting the perturbation parameters). We now set free not only the perturbation parameters r , n_s , $\ln(10^{10}A_s)$, but also the background parameters $\Omega_b h^2$, $\Omega_c h^2$, τ , θ . Together with the WMAP Collaboration [10], we include in the code the external data on H_0 [21],

BAO [21, 22], and SNIa [23]. In addition, we impose a prior on the ‘‘age of the Universe’’ $t_0 \in (10, 20)$ Gyr. The CMB data are used only up to $\ell_{\max} = 100$. We call this set of assumptions the *Case IV*.

The analysis has led us to the following marginalized 1d values of the background parameters:

$$\begin{aligned} \Omega_b h^2 &= 0.02277^{+0.01906}_{-0.01962}, & \Omega_c h^2 &= 0.1246^{+0.0236}_{-0.0229}, \\ \Omega_\Lambda &= 0.712^{+0.039}_{-0.030}, & \tau &= 0.095^{+0.067}_{-0.080}, \end{aligned}$$

They are quite close to the values that we used as fixed parameters in the *Case III*.

As for the perturbation parameters, the 7d ML point was found at

$$r = 0.313, \quad n_s = 1.075, \quad \ln(10^{10}A_s) = 3.026, \quad (14)$$

and $n_t = 0.075$. We also derived the 1d mean results (see also Table II):

$$n_s = 1.064^{+0.055}_{-0.053}, \quad \ln(10^{10}A_s) = 3.049^{+0.083}_{-0.085}. \quad (15)$$

The 1d likelihood functions for n_s and r are plotted by black curves, also marked by (4), in Fig. 1. The distribution for r again, like in the *Case III*, shows a maximum at $r = 0.2$. The 68% and 95% intervals are covered, respectively, by

$$r \in (0, 0.332) \quad \text{and} \quad r \in (0, 0.471). \quad (16)$$

The reported numbers, as well as the shapes of red (*Case III*) and black (*Case IV*) curves in Fig. 1, are pretty close to each other. The more concentrated form of the likelihood function for r depicted by the black curve, as compared with the red curve, is probably the result of removal of artificial covariances between the background and perturbation parameters implicit in the fixed background parameters assumption of the *Case III*. The *Case IV* is superior to the *Case III* in that its assumptions are more general. And, yet, the results for n_s and r turned out to be quite similar. The spread of distributions for r shown by red and black curves is still considerable, and the likelihoods include (barely) the point $r = 0$ in the 68% C.L.. Nevertheless, the red and black curves are very different from the olive curve in Fig. 1 (*Case I*).

The results of the *Case I* are usually interpreted as a nondetection of GW with a firm upper bound on r . In contrast to the *Case I*, the results of data analysis performed along the lines of *Case III*, and especially *Case IV*, justify our previous conclusion, based now on CosmoMC calculations, that there does exist a hint of presence of relic gravitational waves at the level of $r \approx 0.2$. Of course, this is a hint, but not a reliable detection.

TABLE II: Results for n_s and r in Case III and Case IV

	Maximum likelihood		1-d likelihood	
	n_s	r	n_s	r (95%C.L.)
Case III	1.052	0.285	$1.064^{+0.058}_{-0.059}$	$r < 0.843$
Case IV	1.075	0.313	$1.064^{+0.055}_{-0.053}$	$r < 0.471$

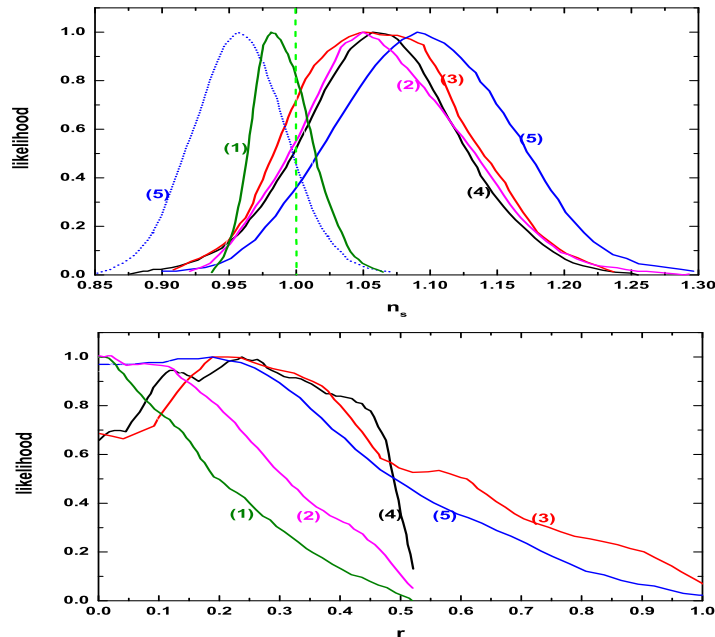


FIG. 1: One-dimensional likelihood functions for n_s (upper panel) and r (lower panel). In both panels, the olive curves, also marked by (1), denote the results for *Case I*, the magenta curves (2) denote the results for *Case II*, the red curves (3) for *Case III*, and the black curves (4) for *Case IV*. In both panels, the blue curves, also marked by (5), denote the results for the *Case V*, i.e. for the case with piecewise power-law spectrum. In the upper panel, the blue solid line (5) shows the likelihood function for $n_s^{(1)}$, whereas the blue dotted line (5) shows the likelihood function for $n_s^{(2)}$. In the lower panel, the blue line (5) shows the likelihood function for r .

IV. JUDGMENTS ABOUT n_s AND r AS FUNCTIONS OF ℓ_{\max}

The assumption of strictly constant spectral indices is a theoretical possibility, but not a necessity, and therefore it should be tested by observations. Here, we show how the judgments about n_s and r depend on the volume of the utilized CMB data. Concretely, we adopt the assumption of constant n_s and n_t , Eq.(2), but we include in the data analysis only the CMB data up to a certain, varied in steps, multipole number ℓ_{\max} : $2 \leq \ell \leq \ell_{\max}$. In other words, the varied ℓ_{\max} of this Section replaces the fixed largest ℓ_{\max} mentioned in Sec.II A.

It would be much too time consuming to run the CosmoMC for each step in ℓ_{\max} . Therefore, for the purpose of this calculation only, we return to the numerical

techniques of Ref. [6]. We set free the perturbation parameters (r , n_s , A_s) and fix the background parameters at the same best-fit WMAP numbers ($\Omega_b h^2 = 0.02260$, $\Omega_c h^2 = 0.1123$, $\Omega_\Lambda = 0.728$, $\tau = 0.087$) that were used in the *Case III* of Sec.III A. The perturbation parameters are being determined from the TT and TE CMB data sets truncated at a given ℓ_{\max} . Since the TT uncertainties are significantly smaller than the TE uncertainties, the major role belongs to the TT data.

The 3d ML values of n_s and r as functions of ℓ_{\max} are shown in Fig. 2. The right panel exhibits the relation between n_s and r which arises when the common variable ℓ_{\max} is excluded. The corresponding marginalized 1d distributions, showing also the 68% uncertainty bars, are plotted in Fig. 3.

It is clearly seen from Fig. 2 and Fig. 3 that when

the ℓ_{\max} is sufficiently large, $\ell_{\max} \geq 350$, the value of n_s approaches $n_s = 0.96$ and r approaches zero. In other words, under the adopted assumptions we recover the results of *Case I* and the conclusions of the WMAP “minimal” model [10]. Specifically, at $\ell_{\max} = 350$ we get the 3d ML values $n_s = 0.963$ and $r = 0.004$.

However, the gradually decreasing ℓ_{\max} leads to the gradually increasing n_s and r . As soon as ℓ_{\max} drops to $\ell_{\max} \approx 160$, the 3d ML points and 1d distributions turn to distinctly blue spectra $n_s > 1$ and nonzero r . At the point $\ell_{\max} = 100$ we return to the 3d ML result of [6]: $n_s = 1.111$ and $r = 0.550$ (equivalent to $R = 0.264$). The sharp drop of r at $\ell_{\max} = 50$ is probably the consequence of small number of participating data points and strongly increased uncertainties, as illustrated in the middle panel of Fig. 3.

As was shown above, within the same assumptions, the CosmoMC technique returns the smaller numbers, $n_s = 1.052$ and $r = 0.285$, at the point $\ell_{\max} = 100$. This was the subject of discussion in *Case III* of Sec.III A. Nevertheless, the general trend toward blue spectra and nonzero r at lower multipoles remains the same, independently of the applied numerical code.

It is interesting to note that the judgments about n_s and r that we arrived at satisfy the linear relations: $r = 0.14 + 3.20(n_s - 1)$ for 3d ML parameters (right panel in Fig. 2) and $r = 0.10 + 3.32(n_s - 1)$ for 1d likelihoods (right panel in Fig. 3). The increased scatter of points at the right ends of these lines is the reflection of increased uncertainties for small values of ℓ_{\max} .

For every fixed ℓ_{\max} , the uncertainties in n_s and r (the vertical bars around central points in the left and middle panels of Fig. 3) can be interpreted as the “degeneracy” between n_s and r , in the sense that one and the same set of data can be quite successfully described by slightly different pairs of n_s and r . For example, at $\ell_{\max} = 100$ (see the left panel in Fig. 2 of Ref.[6]), the “degeneracy” is represented by the more or less elliptical 2d-area, with the major axis providing a linear relation between n_s and r . The movement along this line illustrates the fact that for a given set of data, and at least for $\ell_{\max} = 100$, a slightly larger r requires a slightly larger n_s , and a slightly smaller r requires a slightly smaller n_s . In terms of the left and middle panels of Fig. 3, this would be the movement along the vertical bars around the central point at a given ℓ_{\max} .

It is important to note that the inclined lines in the right panels of Fig. 2 and Fig. 3 have a different meaning. They are the result of movement in the horizontal, rather than vertical, direction, that is, they represent the central values of n_s and r for different sets of data characterized by different limiting ℓ_{\max} . If the hypothesis of a strictly constant n_s (and a fixed r) were true in the entire interval of accessible multipoles, we would expect the inclined lines in the right panels of Fig. 2 and Fig. 3 to degenerate to a point, surrounded by some uncertainties. But this did not happen. We interpret this fact as a hint of a genuine, even if a very simple, dependence of

n_s on spatial scale.

V. PIECEWISE POWER-LAW SPECTRA

The findings described in previous Sections support the proposition that it is unwise to postulate one and the same power-law spectrum of primordial perturbations for all wavelengths covered by the existing data. It is risky to do this independently of the issue of relic gravitational waves. But what is more important for us, we have shown that if this postulate is imposed, any signs of GW in CMB disappear, see Sec.IV and *Case I* in Sec.II A. On the other hand, it is also true that it is easier to demonstrate the drawbacks of a given hypothesis than propose a better one. In the absence of a firm guidance, we will explore the hypothesis which allows the primordial spectrum to consist of two power-law pieces. This means that we adopt the GW and DP power spectra in the form of Eqs.(3)-(6). We want to show that this hypothesis is very much consistent with the indications of GW at lower multipoles, as found in Sec.III, and with the preference for a blue spectrum at longer wavelengths and a red spectrum at shorter wavelengths, as was discussed in Sec.II B and Sec.IV.

To be as close as possible to the already performed calculations, we use $k_1 = 0.01\text{Mpc}^{-1}$ in Eqs.(3)-(6). This choice of k_1 corresponds approximately to the multipole $\ell = 100$ [24]. Certainly, there is no reason for the piecewise spectrum to be discontinuous at the wave number k_1 , and Eqs. (3)-(6) take care of this. In general, the parameters $A_s^{(2)}$ and $A_s^{(1)}$ are not equal to each other, they are linked by the relation shown in Eqs.(3)-(6). [28]

We again use the CosmoMC sampler. The objective is to build the likelihood function in the 8-dimensional parameter space, consisting of four background parameters ($\Omega_b h^2$, $\Omega_c h^2$, τ , θ) and four perturbation parameters ($\ln(10^{10} A_s^{(1)})$, $n_s^{(1)}$, $n_s^{(2)}$, r). The parameter $A_s^{(2)}$ is expressible in terms of $A_s^{(1)}$, while the spectral indices n_s and n_t in both parts of the spectrum are related by $n_t = n_s - 1$. The parameters $n_s^{(1)}$ and $n_s^{(2)}$ are not necessarily different; it is the maximum likelihood analysis of the data that will tell us their preferred values. Obviously, if it is postulated that $n_s^{(1)} \equiv n_s^{(2)}$, or if it happens that $n_s^{(1)} = n_s^{(2)}$ in a particular realization of random trials, then we simply return to the outcomes of the already considered *Case I* in Sec.II A. We call the introduced set of assumptions the *Case V*.

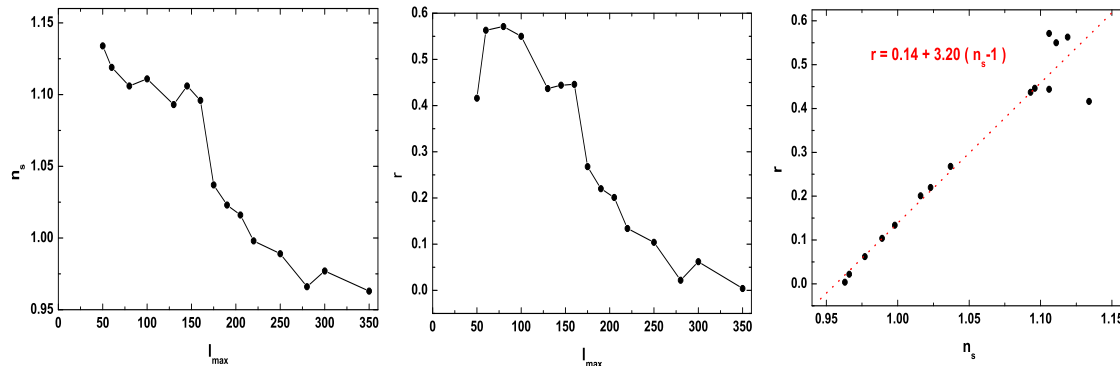
We again take into account all the WMAP7 data for TT , TE , EE and BB correlation functions in the interval $2 \leq \ell \leq \ell_{\max}$, where $\ell_{\max} = 1200$ for TT , 800 for TE , and 23 for EE and BB . The 8d maximum likelihood values of the parameters r , $n_s^{(1)}$, $n_s^{(2)}$ in the *Case V* are found to be

$$r = 0.113, \quad n_s^{(1)} = 1.067, \quad n_s^{(2)} = 0.936. \quad (17)$$

The marginalized 1d likelihood functions for these three

TABLE III: Results for $n_s^{(1)}$, $n_s^{(2)}$ and r in Case V

	Maximum likelihood			1-d likelihood		
	$n_s^{(1)}$	$n_s^{(2)}$	r	$n_s^{(1)}$	$n_s^{(2)}$	r (95% C.L.)
Case V	1.067	0.936	0.113	$1.095^{+0.062}_{-0.061}$	$0.958^{+0.032}_{-0.032}$	$r < 0.720$

FIG. 2: The maximum likelihood values of n_s and r as functions of l_{\max} .

parameters are plotted in Fig. 1 by blue curves, also marked by symbol (5). The 1d results, including the 68% uncertainties, can be summarized as follows (see also Table III),

$$n_s^{(1)} = 1.095^{+0.062}_{-0.061}, \quad n_s^{(2)} = 0.958^{+0.032}_{-0.032}, \quad r \in (0, 0.383)_{18}$$

Examining the numerical results (17), (18) and blue curves (5) in Fig. 1 we can conclude the following. First, the values for $n_s^{(1)} > 1$ and $n_s^{(2)} < 1$ confirm the expectation that the preferred shapes of primordial spectra are blue at long wavelengths and red at short wavelengths. The larger (blue) index $n_s^{(1)}$ minus its 1σ does not overlap with the smaller (red) index $n_s^{(2)}$ plus its 1σ . The value of the (blue) index $n_s^{(1)}$ is about the same as the values for n_s found in the *Case III* and in the *Case IV* for the interval $2 \leq \ell \leq 100$. And the value of the (red) index $n_s^{(2)} = 0.958$ is about the same (slightly less) than $n_s = 0.969$ found in [6] for the interval $101 \leq \ell \leq 220$.

The general shape of the likelihood function for r (blue curve (5) in the lower panel of Fig. 1) is quite similar to the distributions (3) and (4), plus the expected flattening of the likelihood function (5) at small values of r . The flattening is expected because there is still a large area in the parameter space where $n_s^{(1)}$ is equal to $n_s^{(2)}$ and both

of them are less than 1, see the likelihoods (5) in the upper panel of Fig. 1. As we know from the analysis of the *Case I* all these options return very small values of the parameter r . This is why the probability of small values of r has increased in comparison with the “clean” cases, *Case III* and *Case IV*, and the likelihood function (5) has flattened and became consistent with the hypothesis of no gravitational waves, $r = 0$.

The hypothesis of a piecewise spectrum (*Case V*) is pretty much in agreement with WMAP7 data and with all other findings discussed here. But it also illustrates how careful one should be in judgments about the absence or presence of gravitational waves in CMB data. Hopefully, the forthcoming data of better quality will allow us to make more decisive conclusions.

VI. PROJECTIONS ON THE PLANCK MISSION

The CosmoMC calculations have tempered our previous evaluations [6] of relic GW in WMAP7 data. The indications became weaker, but we do not think they disappeared altogether. The projections on the possible Planck findings are anticipated to become worse, but it is important to see what they are now. The GW sig-

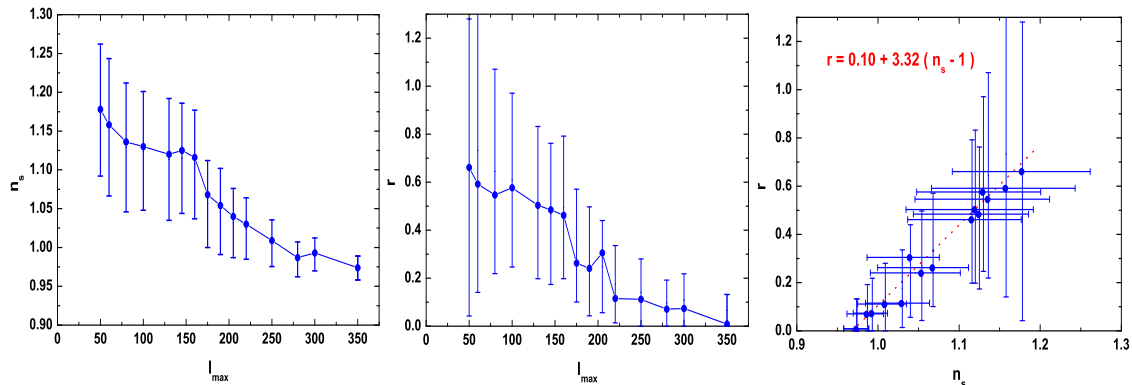


FIG. 3: The marginalized One-dimensional distributions (constraints) of n_s and r as functions of l_{\max} . The vertical bars denote the uncertainties at 68% C.L.

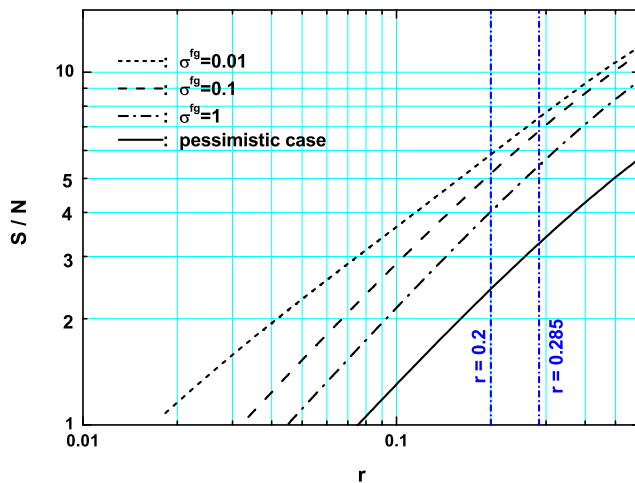


FIG. 4: The Planck's signal-to-noise ratio S/N for expected GW signals considered in the text.

nal may have declined in strength, but the good news is that Planck is definitely expected to operate for 28 months rather than for 14 months. The longer duration of observations will partially compensate the suspected weakening of the GW signal.

Following [6], we use the signal-to-noise ratio

$$\frac{S}{N} \equiv \frac{r}{\Delta r}, \quad (19)$$

where the uncertainty Δr depends on statistics and various instrumental and environmental noises. All our input assumptions about Planck's instrumental noises, number

and specification of frequency channels, foreground models and residual contamination, sky coverage, etc., are exactly the same as in our previous papers [6]. In particular, the ability, ranging from excellent to none, of removing the foreground contamination is characterized by the parameter $\sigma^{\text{fg}} = 0.01, 0.1, 1$. We also work with the pessimistic case, in which $\sigma^{\text{fg}} = 1$ and the nominal instrumental noise in the BB information channel at each frequency is increased by a factor of 4.

The uncertainty Δr is evaluated with the help of the Fisher matrix formalism [26]. Since all three perturbation parameters r , n_s and A_s are supposed to be determined from the same set of Planck's data at $2 \leq \ell \leq 100$, we calculate the rr -element of the inverse Fisher matrix, $\Delta r = \sqrt{(F^{-1})_{rr}}$. All information channels, i.e. TT , TE , EE and BB correlation functions, are taken into account. The data from the frequency channels at 100, 143, and 217 GHz are supposed to be used, and the observation time of the Planck mission is taken as 28 months.

We illustrate in Fig. 4 the results of the revised calculation of S/N as a function of r . The two benchmark values of r derived from the CosmoMC analysis are shown: $r = 0.285$, which is the ML value of r found in the *Case III*, and $r = 0.2$, which is the 1d peak value of r , which is found in the *Case III* and *Case IV*. Assuming that $r = 0.285$ or $r = 0.2$ are fair representations of the reality, the prospects of discovering relic gravitational waves with Planck are still encouraging.

If the true value of the parameter r is $r = 0.285$, the S/N becomes $S/N = 7.43, 6.81, 5.43$ for $\sigma^{\text{fg}} = 0.01, 0.1, 1$, respectively. Even in the pessimistic case, the detection looks quite confident, because the expected level is $S/N = 3.27$. On the other hand, if $r = 0.2$ is the true value of r , the S/N diminishes to $S/N = 5.87, 5.19, 4.05$ for $\sigma^{\text{fg}} = 0.01, 0.1, 1$, respectively. In the pessimistic case, the prospects of detection drop to $S/N = 2.45$.

To conclude, the CosmoMC-revised values of r make the forecasts for the Planck mission worse than previously evaluated in [6]. It looks like some luck will be needed

in the context of the foreground removal. Nevertheless, even in the pessimistic scenario, the S/N remains at the interesting level $S/N > 2$. It is also necessary to remember that the search specifically for the B-mode of CMB polarization by the ground-based and suborbital experiments (see, for example [27]) provides an important extra avenue for the detection of relic gravitational waves.

VII. CONCLUSIONS

We have reanalyzed the WMAP7 data with the help of CosmoMC package and have shown that the (marginal) indications of relic gravitational waves are still present. It is vitally important not to overlook relic GW in the forthcoming data of better quality. The GW signal is weak and its discovery can be done, realistically, only by parametric methods. Therefore, a correct theoretical model and adequate data analysis techniques are especially crucial. We have stressed the importance of looking for GW in the lower- ℓ interval of multipoles and the dangers of unwarranted assumptions about density perturbations. The imminent release of the results of Planck observations will hopefully confirm our expectations.

Acknowledgements

We acknowledge the use of the Legacy Archive for Microwave Background Data Analysis (LAMBDA) [14] and the CosmoMC package [13]. Numerical calculations have been done at the facilities of Niels Bohr Institute and Danish Discovery Center. We are very grateful to P.Naselsky and J.Kim for invaluable help in CosmoMC analysis and discussions. W.Z. is partially supported by Chinese NSF Grants No. 10703005, No. 10775119 and No. 11075141. We thank the anonymous referee for useful comments.

-
- [1] S.W.Hawking and G.Ellis, *The Large Scale Structure of Space-Time* (Cambridge University Press, Cambridge, England, 1973).
 - [2] Ya.B.Zeldovich, *Pis'ma JETP* **7**, 579 (1981); L.P.Grishchuk and Ya.B.Zeldovich, in *Quantum Structure of Space and Time*, Eds. M.Duff and C.Isham, (Cambridge University Press, Cambridge, England, 1982), p. 409; Ya.B.Zeldovich, *Cosmological field theory for observational astronomers*, *Sov. Sci. Rev. E Astrophys. Space Phys.*, Harwood Academic Publishers, Vol. 5, pp. 1-37 (1986) (http://nedwww.ipac.caltech.edu/level5/Zeldovich/Zel_contents.html); A.Vilenkin, in "The Future of Theoretical Physics and Cosmology", Eds. G.W.Gibbons, E.P.S.Shellard and S.J.Rankin (Cambridge University Press, Cambridge, England 2003); L.P.Grishchuk, *Space Science Reviews* **148**, 315 (2009) [arXiv:0903.4395].
 - [3] A.H.Guth, *Phys. Rev. D* **23**, 347 (1981); A.D.Linde, *Phys. Lett.* **B108**, 389 (1982); A.Albrecht and P.J.Steinhardt, *Phys. Rev. Lett.* **48**, 1220 (1982).
 - [4] A.A.Starobinsky, *Phys. Lett.* **B91**, 99 (1980).
 - [5] L.P.Grishchuk, *Sov. Phys. JETP* **40**, 409 (1975); *Ann. N. Y. Acad. Sci.* **302**, 439 (1977); *JETP Lett.* **23**, 293 (1976) (http://www.jetpletters.ac.ru/ps/1801/article_27514.pdf); *Sov. Phys. Usp.* **20**, 319 (1977); in *General Relativity and John Archibald Wheeler*, Eds. I.Ciufolini and R.Matzner, (Springer, New York, 2010) pp. 151-199 [arXiv:0707.3319].
 - [6] W.Zhao, D.Baskaran, and L.P.Grishchuk, *Phys. Rev. D* **82**, 043003 (2010).
 - [7] L.P.Grishchuk and M.Solokhin, *Phys. Rev. D* **43**, 2566 (1991).
 - [8] A.Kosowsky and M.S.Turner, *Phys. Rev. D* **52**, R1739

- (1995).
- [9] V.F.Mukhanov, H.A.Feldman, and R.H.Brandenberger, Phys. Rep. **215**, 203 (1992); D.H.Lyth and A.Riotto, Phys. Rep. **314**, 1 (1999).
- [10] E.Komatsu et al., arXiv:1001.4538.
- [11] D.Larson et al., arXiv:1001.4635.
- [12] Planck Collaboration, arXiv:astro-ph/0604069.
- [13] A.Lewis, A.Challinor and A.Lasenby, Astrophys. J. **538**, 473 (2000); A.Lewis and S.Bridle, Phys. Rev. **D66**, 103511 (2002); <http://cosmologist.info/cosmomc/>.
- [14] <http://lambda.gsfc.nasa.gov/>.
- [15] J.R.Pritchard and M.Kamionkowski, Ann. Phys. (N.Y.) **318**, 2 (2005); W.Zhao and Y.Zhang, Phys. Rev. **D74**, 083006 (2006); D.Baskaran, L.P.Grishchuk and A.G.Polnarev, Phys. Rev. **D74**, 083008 (2006); T.Y.Xia and Y.Zhang, Phys. Rev. **D78**, 123005 (2008).
- [16] P.Vielva, E.Martinez-Gonzalez, R.B.Barreiro, J.L.Sanz and L.Cayon, Astrophys. J. **609**, 22 (2004); M.Cruz, N.Turok, P.Viela, E.Martinez-Gonzalez and M.Hobson, Science **318**, 1612 (2007); P.Naselsky, P.R.Christensen, P.Coles, O.Verkhodanov, D.Novikov and J.Kim, arXiv:0712.1118.
- [17] M.Tegmark, A.de Oliveira-Costa and A.J.S.Hamilton, Phys. Rev. **D68**, 123523 (2003); D.J.Schwarz, G.D.Starkman, D.Huterer and C.J.Copi, Phys. Rev. Lett. **93**, 221301 (2004); K.Land and J.Magueijo, Mon. Not. Roy. Astron. Soc. **357**, 994 (2005); Phys. Rev. **D72**, 101302 (2005); C.L.Bennett et al., arXiv:1001.4758.
- [18] K.Land and J.Magueijo, Phys. Rev. **D72**, 101302 (2005); J.Kim and P.Naselsky, Astrophys. J. Lett. **714**, L265 (2010); Phys. Rev. **D82**, 063002 (2010); Astrophys. J. Lett. **724**, L217 (2010).
- [19] M.Zaldarriaga and U.Seljak, Phys. Rev. **D55**, 1830 (1997); M.Kamionkowski, A.Kosowsky and A.Stebbins, Phys. Rev. **D55**, 7368 (1997).
- [20] W.Zhao, D.Baskaran, and L.P.Grishchuk, Phys. Rev. **D79**, 023002 (2009).
- [21] A.G.Riess et al., Astrophys. J. **699**, 539 (2009).
- [22] W.J.Percival et al., Mon. Not. Roy. Astron. Soc. **401**, 2148 (2010).
- [23] M.Hicken et al., Astrophys. J. **700**, 1097 (2009); M.Kowalski et al., Astrophys. J. **686**, 749 (2008).
- [24] W.Zhao and D.Baskaran, Phys. Rev. **D79**, 083003 (2009).
- [25] E.Gjerlow and O.Elgaroy, arXiv:1008.4471.
- [26] M.Tegmark, A.Taylor and A.Heavens, Astrophys. J. **480**, 22 (1997); M.Zaldarriaga, D.Spergel and U.Seljak, Astrophys. J. **488**, 1 (1997); D.J.Eisenstein, W.Hu and M.Tegmark, Astrophys. J. **518**, 2 (1999).
- [27] H.C.Chiang et al., Astrophys. J. **711**, 1123 (2010).
- [28] In contrast, the recent paper [25] explores, possibly due to an oversight, a strange discontinuous spectrum, where the spectral index n_s is taken as a “steplike” index, but the parameter A_s is one and the same in both pieces of the spectrum.